$$\begin{cases} a_s u_s' = a_{ss} u_{ss}' + a_n u_n' + a_l u_l' + a_m u_m' + a_h u_h' + a_j u_j' + \left(p_P' - p_S'\right) A_s \\ a_e v_e' = a_{se} v_{se}' + a_{ne} v_{ne}' + a_{ee} v_{ee}' + a_w v_w' + a_d v_d' + a_i v_i' + \left(p_P' - p_E'\right) A_e \\ a_t w_t' = a_{st} w_{st}' + a_{nt} w_{nt}' + a_c w_c' + a_k w_k' + a_{tt} w_{tt}' + a_b w_b' + \left(p_P' - p_T'\right) A_t \end{cases} \quad (16)$$

where relations (14) and (15) where taken into account, and: $A_s=dydz$, $A_e=dxdz$, $A_t=dxdy$

For the calculation of speed corrections obtained with equations (16) we used the SIMPLE procedure. The method is called semi-default because the terms containing speed corrections from the neighboring grid points are omitted, thus the correction speeds became:

$$\begin{cases} a_s u_s' = \left(p_P' - p_S'\right) A_s \\ a_e v_e' = \left(p_P' - p_E'\right) A_e \\ a_t w_t' = \left(p_P' - p_T'\right) A_t \end{cases} \quad (17) \qquad \text{or} \qquad \begin{cases} u_s' = d_s \left(p_P' - p_S'\right) \\ v_e' = d_e \left(p_P' - p_E'\right) \\ w_t' = d_t \left(p_P' - p_T'\right) \end{cases} \quad (18)$$

where we noted: $d_s = \dfrac{A_s}{a_s}, \quad d_e = \dfrac{A_e}{a_e}, \quad d_t = \dfrac{A_t}{a_t}$

Correct speeds are given by:

$$\begin{cases} u_s = u_s^* + d_s \left(p_P' - p_S'\right) \\ v_e = v_e^* + d_e \left(p_P' - p_E'\right) \\ w_t = w_t^* + d_t \left(p_P' - p_T'\right) \end{cases} \quad (19)$$

2.5 Establishing the correct pressure equation

The continuity equation (4) was integrated on the control volume centered in point *P* (Fig. 4), obtaining:

$$\left(\rho_p - \rho_p^0\right)\frac{V}{dt} + \left[(\rho u)_s - (\rho u)_n\right]dydz + \left[(\rho v)_e - (\rho v)_w\right]dxdz + \left[(\rho w)_t - (\rho w)_b\right]dxdy = 0 \quad (20)$$

By substituting the corrected speeds, relations (19) in equation (20) we obtain:

$$\begin{aligned} &\left(\rho_P - \rho_P^0\right)\frac{V}{dt} + \left[\left(\rho u^*\right)_s + \rho_s d_s \left(p_P' - p_S'\right) - \left(\rho u^*\right)_n - \rho_n d_n \left(p_N' - p_P'\right)\right]dydz + \\ &+ \left[\left(\rho v^*\right)_e + \rho_e d_e \left(p_P' - p_E'\right) - \left(\rho v^*\right)_w - \rho_w d_w \left(p_W' - p_P'\right)\right]dxd + \\ &+ \left[\left(\rho w^*\right)_t + \rho_t d_t \left(p_P' - p_T'\right) - \left(\rho w^*\right)_b - \rho_b d_b \left(p_B' - p_P'\right)\right]dxdy = 0 \end{aligned} \quad (21)$$

and regrouping the terms we have:

$$a_p p_p' = a_s p_S' + a_N p_N' + a_E p_E' + a_W p_W' + a_T p_T' + a_B p_S' + b \quad (22)$$

where we noted:

$$a_S = \rho_s d_s dydz, \; a_N = \rho_n d_n dydz, \; a_E = \rho_e d_e dxdz, \; a_W = \rho_w d_w dxdz, \; a_T = \rho_t d_t dxdy, \; a_B = \rho_b d_b dxdy \quad (23)$$

$$a_P = a_S + a_N + a_E + a_W + a_T + a_B \quad (24)$$

$$b = \left(\rho_P^0 - \rho_P\right)\frac{V}{dt} + \left[\left(\rho u^*\right)_n - \left(\rho u^*\right)_s\right]dydz + \left[\left(\rho v^*\right)_w - \left(\rho v^*\right)_e\right]dxdz + \left[\left(\rho w^*\right)_b - \left(\rho w^*\right)_t\right]dxdy \quad (25)$$

It should be noted that, although the notations of the coefficients resemble the notations used in the discretization of the heat conservation equation, here they have a completely different meaning (pressure).

In this context we have seen a lot of interests in the literature about the experimental and theoretical investigation of the heat pipes. [25-28]

3 Results and discussion

For the analysis of the flow and heat transfer phenomena in the upper compartment was used a spatial grid with steps *dx=dy=0.002 m* and *dz=0.004 m*, resulting a number of *im x jm x km = 383 x 46 x 78 = 1374204* computational cells. But observing that the vertical median plane – perpendicular on the wall that contains input and output orifices from the upper compartment – parallel with lateral walls, is a symmetry plane, number of computational cells was reduced in half by replacing *jm=46* cu *jm=23*, resulting a number of *687102* cells.

Required temperatures: lower wall of upper compartment $t_{inf}=29°C$, wall of heat pipes at constant temperature of $t_{pipe}=32°C$. To take account of heat losses at the interface with the environment, an additional layer of air was added near the lateral faces and the upper face of the compartment, with a constant temperature of t_{air} = *22°C*.

Thermophysical characteristics of materials that are part of the upper compartment are shown in Table 1.

Table 1. Thermophysical characteristics of materials.

Thermophysical characteristic	Value
Water density, ρ_{water}	977 kg/m^3
Specific heat of water, c_{water}	4180 J/kg°C
Thermal conductivity coefficient of water, k_{water}	0.61 W/m°C
Cinematic water viscosity, μ	0.8 x 10^{-6} m^2/s
Thermal expansion coefficient of water, β	0.000207°C^{-1}
Steel density, ρ_{steel}	7800 kg/m^3
Specific heat of steel, c_{steel}	630 J/kg °C
Thermal conductivity coefficient of steel, k_{steel}	60 W/m °C
Copper density, ρ_{copper}	8920 kg/m^3
Specific heat of copper c_{copper}	390 J/kg °C
Thermal conductivity coefficient of copper, k_{copper}	399 W/m °C
Speed of water input, $v_{w.i.}$	0.27 m/s

Values of the parameters used for the initial conditions are shown in Table 2. Two runs were performed and for each of them the initial condition varied:

Table 2. Initial conditions used for each run.

Run no.	D_0 [m³/h]	$v_{w.i.}$ [m/s]	t_{air} [°C]	t'_2 [°C]	t'_1 [°C]
1.	0.37	0.083	22	12	35
2.	1.18	0.261	27	22	60

The runs were conducted with a variable time step, determined based on the maximum flow speed at the beginning of each cycle.

The flow divider in the upper compartment has the purpose of increasing the heat exchanger's efficiency, because the main flow passes twice between the condensing sides of the heat pipes [11], thus the cold water will accumulate a larger amount of heat – in a given interval of time.

Figure 8 *a)* and *b)* presents the position of the free surface in vertical transversal sections close to the input orifice, at 10 mm from the wall with the input orifice, and in the section that contains the first two heat pipes. We can see the partially filled cells and the formation of swirling currents near the walls, centered in points *A* and *B*. Also, there are swirling currents formed between pipes and lateral walls.

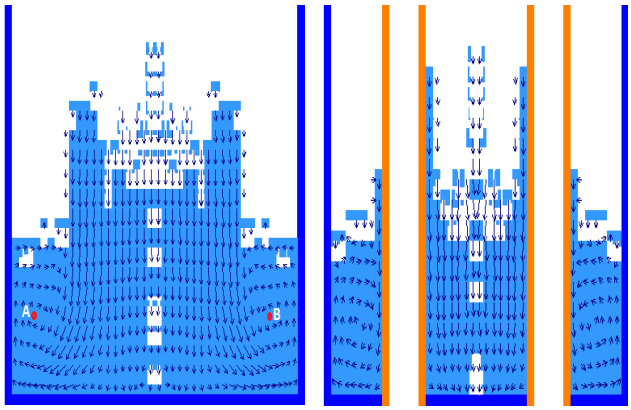

a) *b)*

Fig. 8. Position of the free surface, at $t = 0.24$ *s*, $v_{w.i.} = 0.083$ *m/s*. *a)* in vertical transversal section, at 10 mm from the wall with the input orifice and *b)* in section that contains the first two heat pipes near the input orifice.

Results obtained from running the program, in which the heat exchange is taken into account, are presented below.

In Figure 9 is presented the distribution of temperature in the central vertical section at $t=168$ *s* from the beginning of operation of the heat exchanger and at $t'_1 = 35$°C, $t'_2 = 12$°C, $t_{air} = 22$°C, $v_{w.i.} = 0.083$ *m/s*. Near the lateral walls, the upper wall and in the flow divider plate, the temperature is lower, with values between 13 – 15°C. Near the inferior wall, in contact with the lower compartment and heat pipes, there is a warm layer with temperatures of 25 – 27°C. Inside, there are warmer traces next to the heat pipes. At the left end of the divider plate there is a deformation of these traces, due to a swirling current formed in this phase of operation of the heat exchanger.

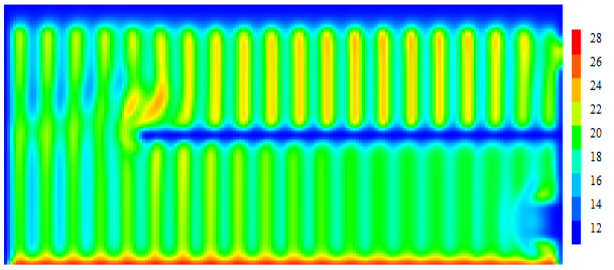

Fig. 9. Distribution of temperature in the central vertical section.

In Figure 10 is shown the intensity of speeds, in horizontal section made a distance of 2 cm from the inferior wall. We can see the main current between the 2 rows of pipes, with maximum speeds in the center of the section, slowing of the flow towards the lateral wall opposed to the input. Speed intensity is lower between two consecutive pipes, but also near the central area of the lateral walls.

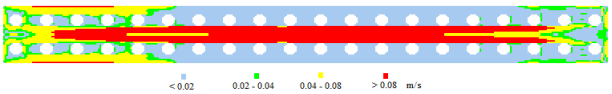

Fig. 10. Intensity of the flow speeds.

Temperature of the preheated water outputting the upper compartment was obtained by a mean of the temperature values in the computational cells, which represent the input sections, namely:

$$T_{output}(t) = \frac{\sum_{i,j,k \in D_{evac}} T[i,j,k]}{N} \tag{26}$$

where: T_{output} is the temperature in the evacuation section; D_{evac} is the domain formed by cells that are part of the evacuation section; t is time that passed since the beginning of operation of the heat exchanger; N is the number of computational cells in the evacuation section.

$T_{ies}(t)$ values were saved every step of time and based on these values were constructed graphs of temperature evolution in the evacuation section. In analogy, was determined the mean pressure in the input sections p_{input} and in the evacuation sections p_{output}, in order to determine the pressure drop between the input orifice and the evacuation orifice:

$$\Delta p = p_{input} - p_{output} \tag{27}$$

In Figure 11 are presented the variation of temperatures of preheated water, at the output orifice from the upper compartment. We can observe that time required to obtain a state of quasi-stationary state depends of the input speed, initial temperature of the cold water and temperature of the environment. In this figure we can observe how the cold water temperature varies depending on time at the output orifice of the upper compartment in the case of the first run.

Due to the heat insulating paint applied on the lateral and upper walls, the heat exchange coefficient between the walls and the environment have a relatively low

value of 2 W/m^2 °C. At lower input speeds, the quasi-stationary phase is obtained later. Similarly, at lower environment temperatures, the time required to obtain the quasi-stationary state increases.

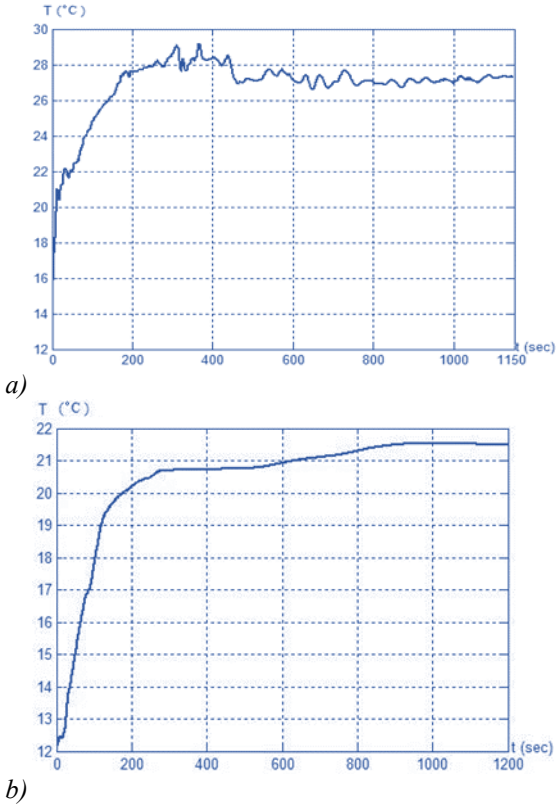

Fig. 11. Variation of temperature of heated water at the output orifice: *a)* first run; *b)* second run.

A centralization of the values obtained for temperature during the two runs, is shown in Table 3. Results obtained for the estimated efficiency are presented in this table based on relation [29].

$$\varepsilon_{estimated} = \frac{t_2'' - t_2'}{t_1' - t_2'} \cdot 100\% \tag{28}$$

where: $\varepsilon_{estimated}$ is the thermal efficiency estimated from the computer simulation; t_2'' is the temperature in the evacuation section; t_2' is the temperature of cold water at the input orifice; t_1' is the temperature of wastewater at the input.

Table 3. Values obtained after running the program.

Run no.	$V_{w.i.}$ [m/s]	t_{air} [°C]	t'_2 [°C]	t'_1 [°C]	t''_2 [°C]	Δp [Pa]	ε_{estim} [%]
1.	0.083	22	12	35	27.6	1931.8	68
2.	0.261	27	22	60	34.11	1962.5	32

We can observe that a maximum efficiency was obtained for run number one, and the lowest efficiency for run number two. The cause of low efficiency for run number two is high input speed, which reduces the contact time of cold water with the heat pipes.

4 Conclusions

The program used in the heat and mass transfer simulation was done in the *Delphi 7* programming language, which is a variant of the Turbo Pascal language. This program contained a series of subprograms for discretization of the domain occupied by the heat exchanger with heat pipes, another subprogram for solving the discretization equations and a third one for post-processing.

Parameters for the flow and heat transfer analysis were chosen to be as close as possible to the real existing conditions, due to the fact that at an experimental level on the laboratory stand we could not use a high enough flow and due to weather conditions (cold water temperature was higher).

The results, obtained by computerized simulation, revealed that the recovered temperature depends greatly on the flow of wastewater and cold water, which validates the experimental results.

Also, the obtained results revealed that the distribution of speed field inside the upper compartment, between the heat pipes, leads to the formation of swirls, where the heat transfer is much lower, due to the way in which the placement of pipes that are in line.

In the context of the above, we can conclude that heat recovery from wastewater in quasi-stationary regime depends on: *the speed of the input cold water, the initial temperature of the cold water and the temperature of the environment*, which was confirmed by the conducted experimental research.

5 Acknowledgements

The results presented in this paper were obtained with the support of the Technical University of Cluj-Napoca. Through the research Contract no. 1994/12.07.2017, CI_2017_IMM_1, Internal Competition CICDI-2017.

References

1. A. Hepbasli, E. Biyik, O. Ekren, H. Gunerhan, M. Araz, J. Energy Conversion and Management **88**, pp. 700–722 (2014)
2. A.R. Mazhar, S. Liu, A. Shukla, J. Energies **11**, 386, pg. 34. (2018)
3. A. Balastov, N. Kachalov, E. Senkiv, O. Kachalova, J. MATEC Web of Conferences **110**, 01008 (2017)
4. M. Omidi, M. Farhadi, M. Jafari, J. Applied Thermal Engineering **110**, pp. 1075–1090 (2017)
5. O. Culha, H. Gunerhan, E. Biyik, O. Ekren A. Hepbasli, J. Energy and Buildings **104**, pp. 215–232 (2015)
6. A. Matveev, D. Zelentsov, A. Louks, J. MATEC Web of Conferences **106**, 06016 (2017)
7. S. Ornelas, S. Sousa, C. Dong, M. Fernelius, M. Hofer, T. Holsclaw, A. Jennison, D. Mai, K. Ninh,

M. Poel, *Mathematical modeling, numerical simulation and statistical optimization of heat pipe design*, (Report of Center for Applied Mathematics, Computation and Statistics Departament of Mathematics, San Jose, CA, pp. 1–37, 2006)
8. M.I. Heredia, J. Siqueiros, J.A. Hernández, D. Juárez-Romero, A. Huicochea, J.G. González-Rodríguez, J. Applied Thermal Engineering **128**, pp. 737–746 (2018)
9. H. Ma, L. Yin, X. Shen, W. Lu, Y. Sun, Y. Zhang, N. Deng, J. Applied Energy **169**, pp. 177–186 (2016)
10. A. Nouri-Borujerdi, M. Layeghi, J. Fluids Engineering, **126**, pp. 442–448 (2004)
11. S. Knudsen, G.L. Morrison, M. Behnia, S. Furbo, J. Solar Energy, **78**, 2, pp. 281–289 (2005)
12. S.F. Tsai, T.W.H. Sheu, J. Computers & Fluids, **27**, 1, pp. 29–46 (1998)
13. D.J. Durrenmatt, O. Wanner, J. Water Research **48**, pp. 548 - 558 (2014)
14. Gupta M, *Numerical Study of Heat Transfer Enhancement in a Plate-Fin Heat Exchanger Using Rectangular Winglet Type Vortex Generator* (Ph.D. Thesis, National Institute of Technology, Kurukshetra, India, 2010)
15. Khan W.A, *Modeling of Fluid Flow and Heat Transfer for Optimization of Pin-Fin Heat Sinks* (Ph.D. Thesis, University of Waterloo, Canada, 2004)
16. Sahiti N, *Thermale and Fluid Dynamic of Pin Fin Heat Transfer Surfaces* (Ph.D. Thesis, Erlangen University, Nürnberg, Germany, 2006)
17. Williamson N.J, *Numerical Modelling of Heat and Mass Transfer and Optimisation of a Natural Draft Wet Cooling Tower* (Ph.D. Thesis, University of Sydney, Australia, 2008)
18. A.A. Ozalp, I.Dincer, International Journal of Thermal Sciences, **49**, pp. 1799–1812 (2010)
19. N.C. Markatos, J. Ironmaking and Steelmaking, **16**, 4, pp. 266–273 (1989)
20. Patankar S.V, *Numerical Heat Transfer and Fluid Flow* (Taylor & Francis, New York, 1980)
21. Olsen N.B, *CFD Algorithms for Hydraulic Engineering* (Norvegian University of Science and Technology, Trondheim, Norway, 2000)
22. C.W. Hirt, B.D, Nichols, J. Computational Physics, **39**, pp. 201–225 (1981)
23. G.Y. Soh, G.H. Yeoh, V. Timchenko, International Journal of Heat and Mass Transfer, **100**, pp. 573–581 (2016)
24. H-J. Laue, H. Kruse, J. Wärmepumpe Aktuell – Informationszentrum Wärmepumpen + Kältetechnik, **8**, 2, pg. 2 (2009)
25. Faghri A, *Heat Pipe Science and Technology* (Taylor & Francis, New York, 1995)
26. X.-S. Yang, M. Karamanoglu, T. Luan, S. Koziel, J. Computational Science **5**, pp. 119–125 (2014)
27. H. Jouhara, S. Almahmoud, A. Chauhan, B. Delpech, G. Bianchi, A. Tassou R. Llera, F. Lago, J.J. Arribas, J. Energy **141**, pp. 1928–1939 (2017)
28. R.T. Dobson, T.M. Harms, *Lumped parameter analysis of closed and open oscillatory heat pipes*, (in: *11th Int. Heat Pipe Conf.* Tokyo, 12–16 September 1999)
29. Proskiw G. 2003, *Design and Analysis of a Residential Greywater Heat Recovery System* (Report Prepared for CANMET Energy Technology Centre, Canada, pg. 4, 5, 52, 2003)